BMC Cancer

RESEARCH Open Access

Multiparametric MRI-based radiomics and clinical nomogram predicts the recurrence of hepatocellular carcinoma after postoperative adjuvant transarterial chemoembolization

Xinyu Guo[1,3†], Jingjing Song[1†], Lingyi Zhu[4], Shuang Liu[1,2], Chaoming Huang[4], Lingling Zhou[1,3], Weiyue Chen[1,2], Guihan Lin[1,2], Zhongwei Zhao[1,2], Jianfei Tu[1,2], Minjiang Chen[1,2], Feng Chen[3], Liyun Zheng[1,2*] and Jiansong Ji[1,2*]

Abstract

Background This study was undertaken to develop and validate a radiomics model based on multiparametric magnetic resonance imaging (MRI) for predicting recurrence in patients with hepatocellular carcinoma (HCC) following postoperative adjuvant transarterial chemoembolization (PA-TACE).

Methods In this retrospective study, 149 HCC patients (81 for training, 36 for internal validation, 32 for external validation) treated with PA-TACE were included in two medical centers. Multiparametric radiomics features were extracted from three MRI sequences. Least absolute shrinkage and selection operator (LASSO)-COX regression was utilized to select radiomics features. Optimal clinical characteristics selected by multivariate Cox analysis were integrated with Rad-score to develop a recurrence-free survival (RFS) prediction model. The model performance was evaluated by time-dependent receiver operating characteristic (ROC) curves, Harrell's concordance index (C-index), and calibration curve.

Results Fifteen optimal radiomic features were selected and the median Rad-score value was 0.434. Multivariate Cox analysis indicated that neutrophil-to-lymphocyte ratio (NLR) (hazard ratio (HR) = 1.49, 95% confidence interval (CI): 1.1–2.1, $P = 0.022$) and tumor size (HR = 1.28, 95% CI: 1.1–1.5, $P = 0.001$) were the independent predictors of RFS after PA-TACE. A combined model was established by integrating Rad-score, NLR, and tumor size in the training cohort (C-index 0.822; 95% CI 0.805–0.861), internal validation cohort (0.823; 95% CI 0.771–0.876) and external validation cohort (0.846; 95% CI 0.768–0.924). The calibration curve exhibited a satisfactory correspondence.

†Xinyu Guo and Jingjing Song contributed equal to this work

*Correspondence:
Liyun Zheng
liyunzheng1025@163.com
Jiansong Ji
jijiansong@zju.edu.cn

Full list of author information is available at the end of the article

Conclusion A multiparametric MRI-based radiomics model can predict RFS of HCC patients receiving PA-TACE and a nomogram can be served as an individualized tool for prognosis.

Keywords Hepatocellular carcinoma, Postoperative adjuvant transarterial chemoembolization, Recurrence, Radiomics, Nomogram

Introduction

Liver cancer is the sixth most common and the third most lethal malignancy globally, with a 5-year survival rate of approximately 18% [1, 2]. Hepatocellular carcinoma (HCC) accounts for over 85% of all liver cancer cases. Radical hepatectomy is the primary curative treatment for HCC. However, the long-term prognosis after liver resection remains unsatisfactory due to a high recurrence rate of approximately 60–70% within 5 years [3, 4]. Postoperative adjuvant therapies such as transarterial chemoembolization (TACE), chemotherapy, are introduced to prolong the long-term survival of patients with HCC after a hepatectomy [5, 6].

Postoperative adjuvant TACE (PA-TACE) has been shown to reduce the risk of recurrence and improve postoperative survival of HCC patients by eliminating micrometastases, residual small lesions, and cancer cells [7, 8, 9].However, not all HCC patients can benefit from PA-TACE owing to tumor heterogeneity, TACE resistance, and damages from TACE like hepatic and immunological functional impairment [10]. Therefore, it is essential to identify optimal candidates who can benefit from PA-TACE. Biomarkers such as micro RNA-4651 [11], Ki67 expression [12, 13], and microscopic vascular invasion [14] have been proposed to predict tumor recurrence after PA-TACE in HCC. However, these tissue-based biomarkers necessitate invasive procedures to obtain tumor samples and fail to adequately capture the spatiotemporal heterogeneity of the tumors. Additionally, multiple clinical factors, such as alpha-fetoprotein (AFP), alanine aminotransferase-to-hemoglobin ratio (AHR), tumor number, tumor size, and imaging features, are likely to predict the HCC recurrence [14, 15, 16, 17]. Indeed, several prediction models based on these clinical factors have demonstrated promising results in estimating the risk of recurrence after PA-TACE [15, 16, 17]. However, they fall short in considering the complex tumor biology, which may lead to a decline in performance. Thus, a comprehensive evaluation avoiding additional tissue damages, and encompassing both complex tumor biology and clinical features is needed.

Radiomics provides a robust method for extracting high-throughput, mineable, and quantitative radiological features [18, 19]. It can also be considered a 'digital biopsy' of tumoral and peritumoral regions, offering non-invasive, reproducible, and comprehensive insight into tumor biology and heterogeneity [20]. Furthermore, accurately integrating radiomic features and clinical characteristics can enhance precision in intricate clinical decision-making [21]. Radiomics has demonstrated the potential to predict treatment response and prognosis for locoregional [22, 23] and systemic therapies [24] in HCC. Study previously reported that a multi-phase, computed tomography (CT)-based radiomics model to predict HCC recurrence after surgical resection was developed and identify high-risk patients who may benefit from PA-TACE [14]. However, the resolution of CT scan in soft tissues is relatively poor, and the information it can provide is still very limited. In comparison to CT, magnetic resonance imaging (MRI) offers superior soft-tissue resolution, nonionizing radiation exposure, and more functional imaging approaches [25]. This capability allows for a more comprehensive and detailed depiction of organizational information. Indeed, MRI-based radiomics models were applied to predicted the efficacy of system or local treatment for cancers [22, 23, 24]. Our previous study also demonstrated that a MRI-based model combined radiomics and clinical factors acts as a new strategy for predicted the recurrence-free survival (RFS) of intermediate and advanced HCC treated with TACE plus RFA [26]. However, the radiomics features are mainly extracted from one or two MRI sequences, either in our studies or in others' studies [22, 26]. Thus, we aim to investigate the ability of multiparametric MRI radiomics to predict recurrence in HCC patients following PA-TACE.

In this study, we have developed and validated a multiparametric MRI-based radiomics model that provides personalized assessments of HCC recurrence risk before treatment, thereby evaluating the feasibility of its clinical application.

Materials and methods

Study population

This study received approval by the Ethical Committee of Lishui Hospital of Zhejiang University and was carried out in accordance with the Declaration of Helsinki. The requirement for informed consent was waived due to the retrospective nature of the research. A total of 380 patients with HCC who underwent PA-TACE within two months after radical hepatectomy from January 2015 to March 2022 were retrospectively inclueded in the two medical centers. A flowchart of patient enrollment is illustrated in the Fig. 1 The inclusion criteria are as follows: (1) pathological diagnosis of HCC; (2) a qualified, contrast-enhanced MRI scan performed within two

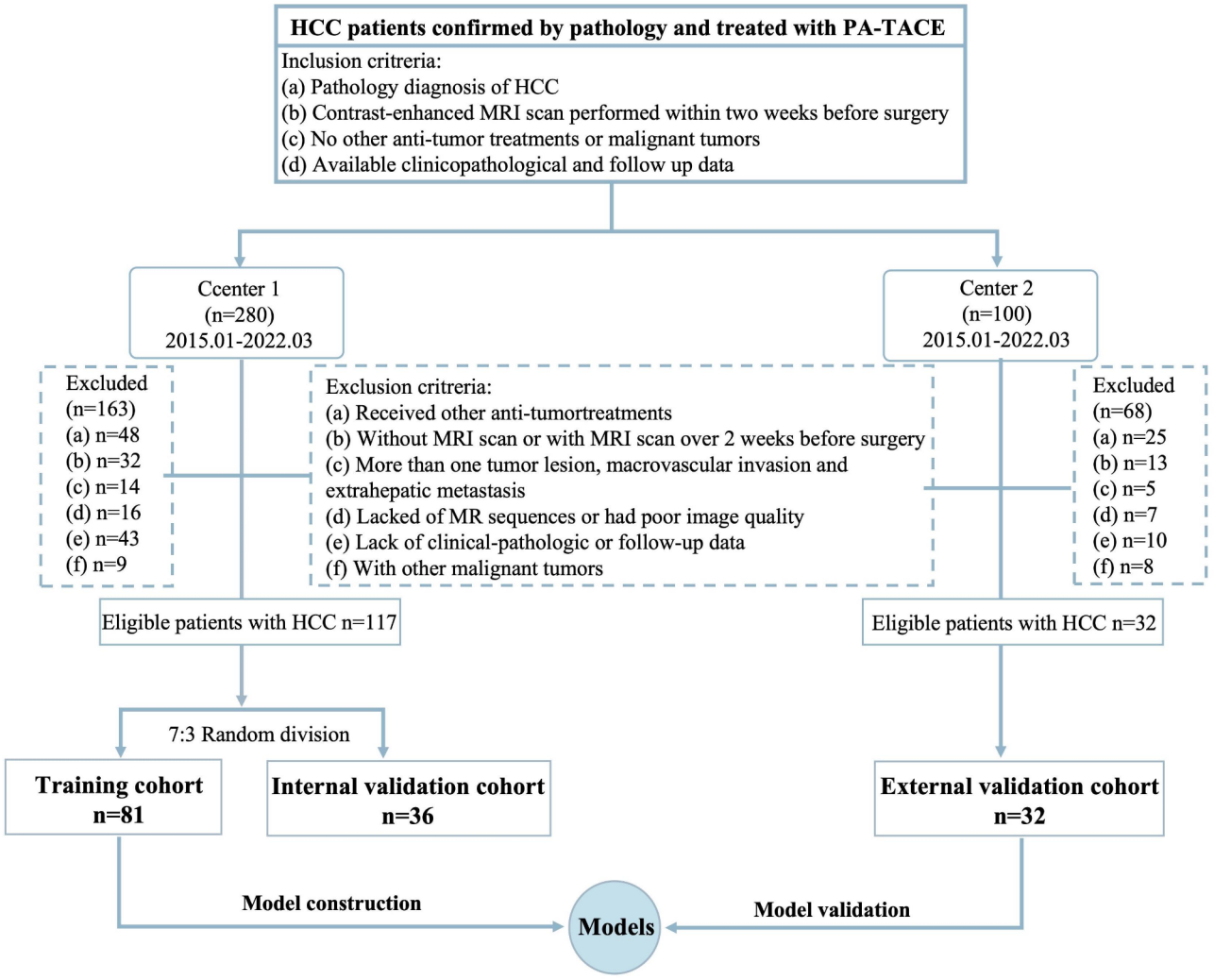

Fig. 1 Flowchart of patients enrollment

weeks before surgery; (3) a follow-up time of more than one year after PA-TACE; (4) no other anti-tumor treatments or malignant tumors. The exclusion criteria were as follows: (1) patients who received other anti-tumor treatments such as radiotherapy, chemotherapy, radiofrequency ablation, or systemic therapy before the hepatectomy; (2) patients without an MRI scan or with an MRI scan more than two weeks before the hepatectomy; (3) patients with more than one tumor lesion, macrovascular invasion, or extrahepatic metastasis; (4) patients who lacked MRI sequences or had poor quality images; (5) patients without clinical-pathology and follow-up data, or with a follow-up time of less than one year after PA-TACE; (6) patients with other malignant tumors. Finally, a total of 149 patients were included in the study. One hundred and seventeen patients from center 1 (Lishui Hospital of Zhejiang University) were selected for inclusion and randomly divided into a training ($n = 81$) and validation cohort ($n = 36$) at a ratio of 7:3. Then, 32 HCC patients from center 2 (the Third Affiliated Hospital of Wenzhou Medical University) were used as an external validation cohort. In addition, clinical factors including patient demographic characteristics; Child-Pugh class clinical grades and Barcelona Clinic Liver Cancer (BCLC) stages, laboratory indicators and histopathological features were collected for further analysis.

Procedure of PA-TACE

Firstly, all included HCC patients underwent R0 hepatectomy, completely resecting the tumor while ensuring tumor-free margins. Then, patients were treated with conventional TACE after hepatectomy with two months. During the performance of PA-TACE, we inserted a hepatic arterial catheter via the femoral artery into the proper hepatic artery using the Seldinger technique. Subsequently, based on a comprehensive evaluation of the patient's body surface area, physical fitness, and residual liver volume, we administered a precisely formulated

mixture of chemotherapeutic agents (fluorouracil, epirubicin, and platinum) and embolic agents (lipiodol and gelatin sponge) through the catheter into the residual liver. When lipiodol deposits were identified during PA-TACE, the angiographic images were independently reviewed by two experienced interventional radiologists. Following PA-TACE procedures, all patients were hospitalized for post-procedural supportive care, and routine management was implemented, encompassing hydration, antiemetic administration, pain control, and continuous monitoring of liver function.

MRI image acquisition and feature evaluation

All MRI scans were performed using a German MAGNETOM Area 1.5T MR scanner (Siemens AG Healthcare, Erlangen, Germany) and a Philips INGENIA 3.0T MR scanner (Philips Medical Systems Nederland B.V.). The detailed parameters of each sequence for the two scanners are shown in Table S1. Preoperative MRI scans were retrospectively evaluated using the Picture Archiving and Communication System (PACS) by two radiologists with 3 and 5 years of experience in liver imaging evaluation, independently. Qualitative and quantitative MRI features were analyzed using the Liver Imaging Reporting and Data System (LI-RADS version 2018) [27]. Detailed definitions of the qualitative features are listed in Table S2.

Follow-up

RFS was the end point of this study. HCC recurrence was screened by monitoring serum AFP levels and identifying new tumor nodules within or outside the liver using contrast-enhanced CT or MRI imaging (Figure S1). RFS was defined as the time from the date of PA-TACE to the date of first recurrence or the last follow-up. The cutoff follow-up date for our research was March 31, 2023.

Image segmentation and feature extraction

The volumes of interest for HCC were manually delineated on T2WI, diffusion-weighted imaging (DWI) (b = 800), and AP using 3D Slicer software (version 4.10, www.slicer.org). The two radiologists independently completed the image segmentations. MRI images were resampled to $1.0 \times 1.0 \times 1.0$ mm^3 voxels using a fixed bin width of 25 to eliminate spatial resolution inconsistencies. Radiomic feature extractions were conducted using PyRadiomics version 3.0.1.

Correlation coefficients (ICCs) were used to evaluate the variability of the extracted features. For the assessment of the intra-observer ICC, MR images of three sequences from 40 patients were randomly selected and segmented twice in one month by one of the radiologists. To assess inter-observer ICC, the randomly selected images underwent independent segmentation by both radiologists. When the ICC exceeded 0.75, it was considered good agreement, and the first radiologist then performed the remaining segmentations.

Feature selection and radiomics model construction

The radiomic features from three sequences were first standardized with z-scores. Next, Least absolute shrinkage and selection operator (LASSO)-COX regression with 10-fold cross validation were used to identify optimal radiomic features. A Rad-score was calculated for each patient through a linear combination of selected feature clusters, with corresponding LASSO coefficients applied as weights (Figure S2). Participants were stratified into high- and low-risk signature groups based on the median value of the Rad-score. The underlying association between the Rad-score and RFS was demonstrated via Kaplan-Meier survival curves in the training and validation cohorts.

Clinical model and combined model building

A clinical model was developed by integrating the optimal clinical factors selected through univariate and multivariate Cox analyses. Then, a combined model was developed to improve prediction performance, we further identified clinical risk factors through and developed a clinical-radiomics nomogram to predict 1-, 3-, and 5-year RFS in both cohorts. Time-dependent receiver operating characteristic (ROC) and calibration curves were used to evaluate the performance of the combined model. The workflow of the radiomics analyses is shown in Fig. 2.

Statistical analyses

Categorical variables were analyzed using the Chi-square test or Fisher's exact test, while continuous variables were analyzed using the Student's t-test or the Mann-Whitney U-test. Survival curves were plotted via the Kaplan-Meier method and compared using the log-rank test. The performance of the combined model was evaluated using time-dependent ROC curves, Harrell's concordance index (C-index), and calibration curves. All statistical analyses were conducted using R software (version 4.1.2). Statistical significance was determined at a p-value<0.05 by all two-sided.

Results

Patient characteristics

A total of 149 HCC patients were included in this study. Among them, 81 patients were classified into the training cohorts, and 36 and 32 patients were classified into the internal and external validation cohorts. The median age of the training cohort was 57.6 years, 70 (86.4%) patients were male, and 49 (60.5%) patients were diagnosed with cirrhosis. The distribution of patients within each BCLC stage was relatively even, with 44.4% at BCLC stage A and

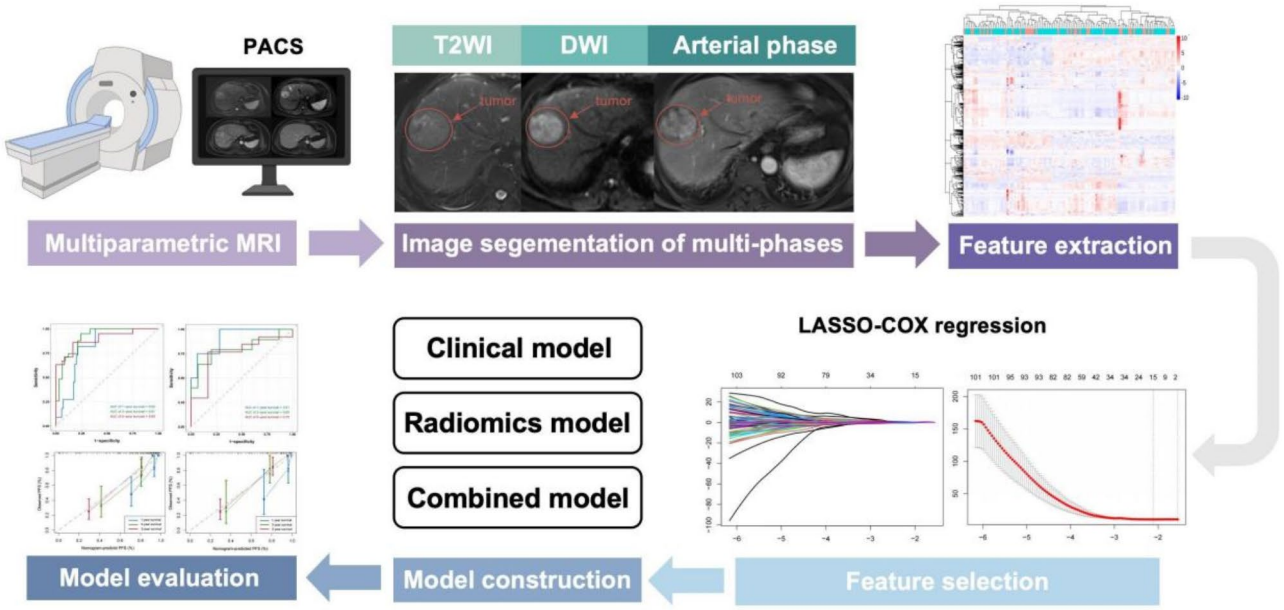

Fig. 2 Workflow of radiomics analysis

55.6% at BCLC stage B. Only 35.8% had undergone antiviral therapy. The overall recurrence rate was 37.6%. Specifically, 35.8%, 44.4% and 34.4% of patients experienced a recurrence after PA-TACE in the training, internal and external validation cohorts and the difference was no significant. Furthermore, there was no significant difference in clinical factors between the training and validation cohorts. The data are summarized in Table 1.

Radiomic features for RFS prediction

The intra- ICCs ranged from 0.81 to 0.93 and inter-observer ICCs ranged from 0.81 to 0.93, demonstrating favorable reproducibility between the two radiologists. Ultimately, 1,688 radiomic features were extracted for each sequence (5,064 in total). The heatmap expressions of extracted radiomic features in each patient are shown in Figure S3. A total of fifteen radiomic features were selected from the 5,064 extracted features to construct the radiomic model: eleven from T2WI, one from DWI, and three from the AP, can be seen in Table S4. A Rad-score was calculated using a formula shown in Table S4, and defined to be 0.434 based on the median value. Kaplan-Meier analysis revealed that patients in high risk group was associated with decreased RFS in training cohort (HR = 12.21, 95% CI: 5.56–26.82, P<0.0001), internal validation cohort (HR = 3.68, 95% CI: 1.38–9.84, P = 0.028) and external validation cohort (HR = 4.63, 95% CI: 1.61–0.92, P = 0.025) (Fig. 3a). The survival trend of OS was consistent with that observed for RFS in the training and validation cohort (Figure S4). Kaplan-Meier analysis indicated that patients in high risk group was associated with decreased OS in training cohort (HR = 5.20, 95% CI: 2.09–12.91, P = 0.008), internal validation cohort (HR = 4.05, 95% CI 1.39–11.78, P = 0.028) and external validation cohort (HR = 4.79, 95% CI: 1.67–13.74, P = 0.021) (Figure S4).

Clinical and radiomic features for RFS prediction

Firstly, Univariate Cox regression analysis reveal that among the 14 clinical factors, only had p values < 0.05(Fig. 4). The three factors with p < 0.05, were subjected to multivariate Cox analysis, and the results suggested that NLR (hazard ratio (HR) = 1.49, 95% confidence interval (CI): 1.10–2.10, P = 0.022), tumor size (HR = 1.28, 95% CI: 1.10–1.50, P = 0.001), and Rad-score (HR = 16.35, 95% CI: 5.90–45.0, P<0.001) were identified as independent predictors of RFS (Table 2). Moreover, the optimal cut off values of NLR and tumor size are calculated using the Kaplan-Meier curves and log-rank test. The cut-off threshold of NLR was 3.0 (Figure S5). Patients in high NLR group was associated with decreased RFS in training cohort (HR = 3.03, 95% CI: 0.95–9.62, P = 0.0048) and internal validation cohort (HR = 3.20, 95% CI: 0.93–10.99, P = 0.014) and external validation (HR = 4.81, 95% CI: 1.20-19.24, P < 0.001) (Fig. 3b). Similarly, the cut-off threshold of tumor size was 4.4 (Figure S6). Patients with high tumor size were associated with worse RFS in training cohort (HR = 2.16, 95% CI: 0.96–4.90, P = 0.034), internal validation cohort (HR = 2.95, 95% CI: 1.06–8.17, P = 0.024) and external validation (HR = 3.53, 95% CI: 1.22–10.23, P = 0.021) (Fig. 3c). Then, a combined model integrating Rad-score and clinical factors was developed.

Table 1 Baseline characteristics of the patients in the training and validation cohorts

	Training (*n* = 81)	**Internal validation (*n* = 36)**	**External validation (*n* = 32)**	***p* value**
Age	57.6 (9.67)	58.3 (8.14)	62.9 (8.46)	0.670
Sex				0.878
Male	70 (86.4%)	30 (83.3%)	26 (81.3%)	
Female	11 (13.6%)	6 (16.7%)	6 (18.7%)	
BMI	23.3 (2.91)	23.7 (3.16)	23.5 (3.16)	0.561
Antiviral treatment				0.961
Absent	52 (64.2%)	24 (66.7%)	11 (34.4%)	
Present	29 (35.8%)	12 (33.3%)	21 (35.6%)	
Cirrhosis				0.563
Absent	32 (39.5%)	17 (47.2%)	10 (31.3%)	
Present	49 (60.5%)	19 (52.8%)	22 (68.7%)	
BCLC stage				0.355
A	36 (44.4%)	12 (33.3%)	20 (62.5%)	
B	45 (55.6%)	24 (66.7%)	12 (37.5%)	
CNLC				0.549
Ia	60 (74.1%)	24 (66.7%)	15 (46.9%)	
Ib	21 (25.9%)	12 (33.3%)	17 (53.1%)	
Child Pugh score				0.661
A5	63 (77.8%)	30 (83.3%)	25 (78.1%)	
A6	18 (22.2%)	6 (16.7%)	7 (21.9%)	
PLT, ×109/L	150 (65.1)	137 (52.4)	182 (61.3)	0.282
ALT, U/mL	32.6 (19.7)	32.8 (26.0)	32.8 (26.0)	0.970
AST, U/mL	31.2 (11.2)	32.6 (14.2)	32.6 (14.2)	0.626
GGT, U/L	64.0 (70.5)	68.9 (65.8)	107 (124)	0.718
ALP, U/L	90.0 (33.7)	89.6 (21.8)	95.0 (36.9)	0.931
TB, umol/L	15.8 (7.58)	15.1 (7.56)	16.3 (7.55)	0.624
CB, umol/L	6.39 (3.07)	6.02 (2.49)	6.02 (2.49)	0.493
ALB, g/L	39.0 (4.13)	40.7 (4.69)	41.9 (3.48)	0.069
PT, second	12.0 (0.93)	11.9 (1.16)	12.1 (0.82)	0.532
INR	1.09 (0.09)	1.07 (0.11)	1.07 (0.11)	0.304
FDP, g/L	2.85 (0.77)	2.93 (0.73)	3.05 (0.94)	0.568
AFP, ng/mL	271 (588)	329 (630)	312 (1216)	0.642
CEA, mg/L	3.06 (1.79)	3.24 (2.19)	2.28 (1.21)	0.654
NLR	2.26 (1.24)	2.39 (1.24)	2.43 (1.70)	0.604
PLR	101 (42.7)	95.8 (33.6)	110 (41.4)	0.484
MLR	0.27 (0.10)	0.30 (0.12)	0.32 (0.19)	0.159
AGLR	142 (101)	140 (57.4)	116 (66.7)	0.903
AHR	0.23 (0.15)	0.23 (0.17)	0.23 (0.17)	0.840
Differentiation degree				0.661
High	14 (17.3%)	4 (11.1%)	4 (12.5%)	
Median	44 (54.3%)	20 (55.6%)	18 (56.3%)	
Low	23 (28.4%)	12 (33.3%)	10 (31.2%)	
Hep expression				0.091
Negative	5 (6.17%)	6 (16.7%)	4 (12.5%)	
Positive	76 (93.8%)	30 (83.3%)	28 (87.5%)	
AFP expression				0.934
Negative	54 (66.7%)	25 (69.4%)	23 (71.9%)	
Positive	27 (33.3%)	11 (30.6%)	9 (28.1%)	
GPC3 expression				1.000
Negative	44 (54.3%)	20 (55.6%)	18 (56.3%)	
Positive	37 (45.7%)	16 (44.4%)	14 (43.7%)	
Ki-67				0.678

Table 1 (continued)

	Training (*n* = 81)	Internal validation (*n* = 36)	External validation (*n* = 32)	*p* value
Low expression	18 (22.2%)	10 (27.8%)	10 (31.3%)	
High expression	63 (77.8%)	26 (72.2%)	22 (68.7%)	
Status				0.496
Non-recurrence	52 (64.2%)	20 (55.6%)	21 (65.6%)	
Recurrence	29 (35.8%)	16 (44.4%)	11 (34.4%)	

BMI, body mass index; BCLC, Barcelona Clinic Liver Cancer; CNLC, China liver cancer staging; PLT, platelet count; ALT, alanine aminotransferase; AST, aspartate aminotransferase; GGT, glutamyl transpeptidase; TB, total bilirubin; CB; conjugated bilirubin; ALB, albumin; PT, prothrombin time; INR, international normalized ratio; FDP, fibrinogen degradation product; AFP, alpha-fetoprotein; CEA, carcinoembryonic antigen; NLR, neutrophil-lymphocyteratio; PLR, platelet-lymphocyte ratio; MLR, lymphocyte-monocyte ratio; AGLR, (ALP [U/L] + GGT[U/L]) /lymphocyte count (×109/L) ratio; AHR, alanine aminotransferase to hemoglobin ratio

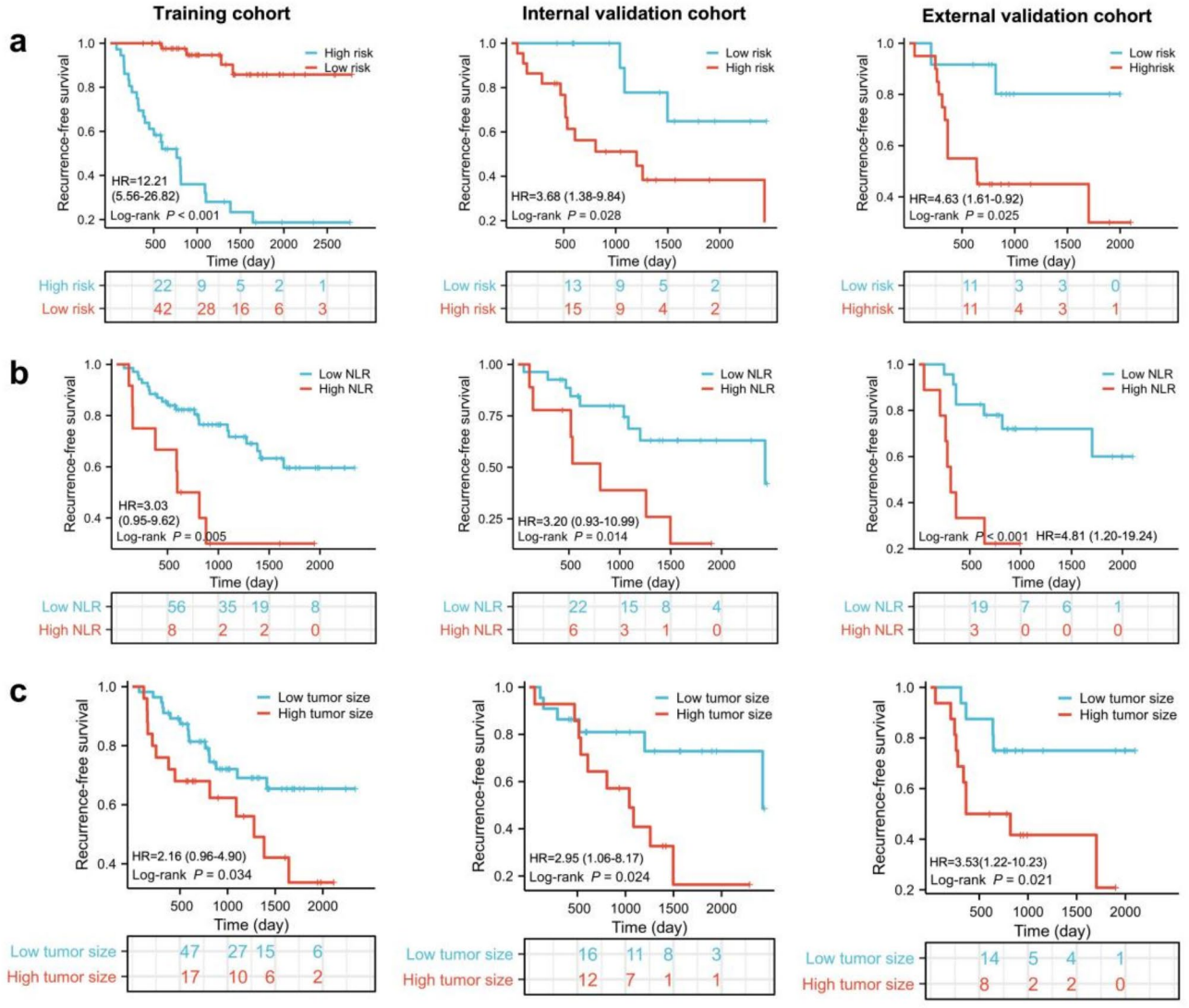

Fig. 3 Kaplan-Meier survival curves based on Rad-score, NLR and tumor size in the training, internal validation and external cohorts. **(a)** Kaplan-Meier survival analysis based on Rad-score. **(b)** Kaplan-Meier survival analysis based on NLR. **(c)** Kaplan-Meier survival analysis based on tumor size

Accuracy of RFS-predictive models

The performance of the different model was compared using the areas under the curve (AUCs) at 1, 3 and 5 years of time-dependent ROC curves. The AUC of radiomics model was 0.84, 0.87 and 0.88 in the training cohorts and the AUCs of clinical model the at 1, 3 and 5 years were 0.53, 0.61 and 0.63. It is notable that the RFS prediction performance of radiomics model is better than that of clinical model. Furthermore, the AUCs of combined model at 1, 3 and 5 years were 0.82, 0.89 and

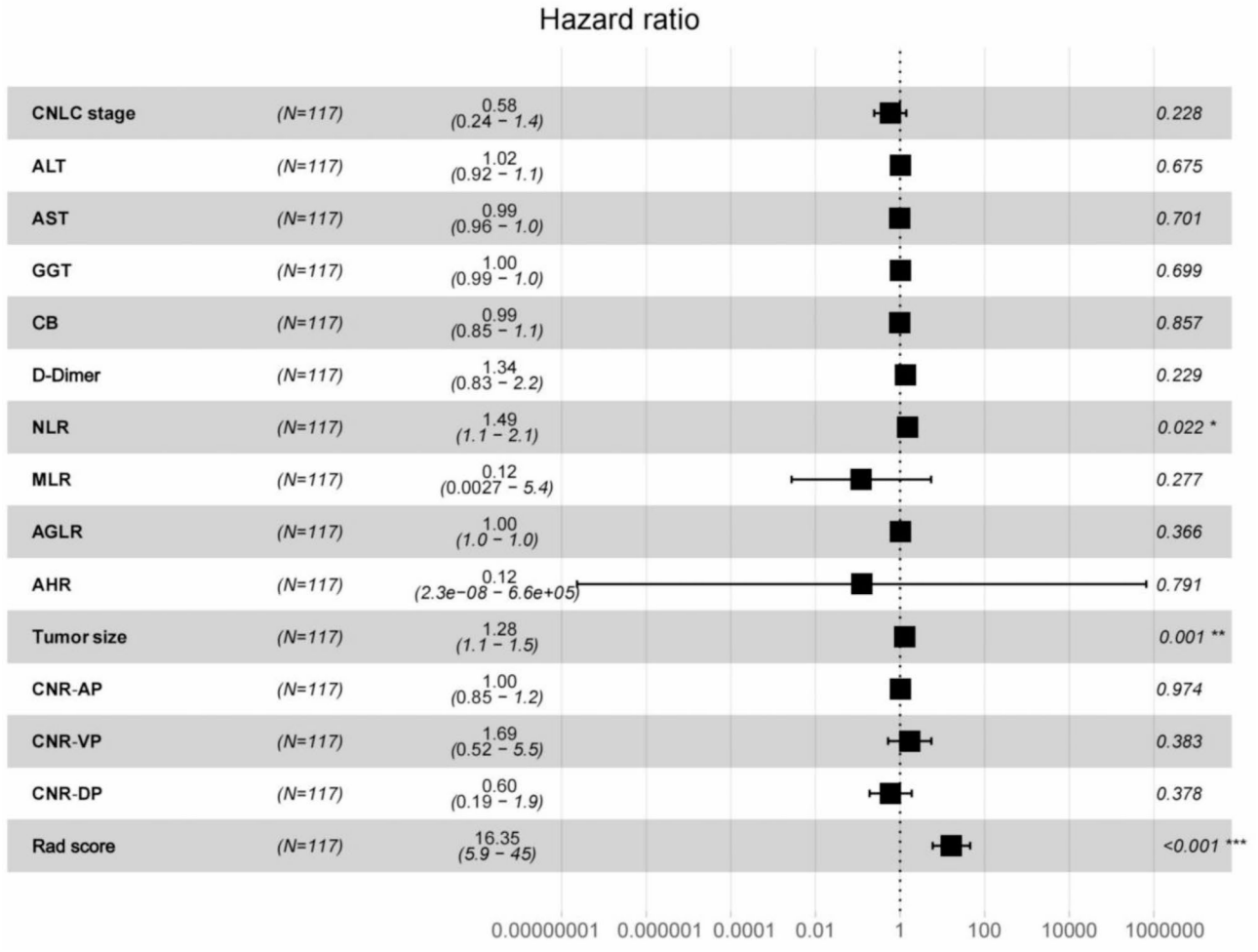

Fig. 4 Multivariable Cox analyses of RFS

Table 2 Multivariable Cox analyses of RFS

	Multivariable analysis		
	Hazard ratio	**95% CI**	***P* value**
NLR	1.49	1.10–2.10	0.022
Tumor size	1.28	1.10–1.50	0.001
Rad score	16.35	5.90–45.0	<0.001

NLR, neutrophil-lymphocyteratio

0.91, demonstrating better RFS prediction performance than clinical model or radiomic model. Similar trend was observed in the internal and external validation cohorts, shown in Fig. 5.

A nomogram for individualized prediction of RFS

To predicted the RFS individually, a novel clinical-radiomic nomogram was constructed based on the Rad-score and two clinical predictors (Fig. 6a). The calibration curve of the clinical-radiomic nomogram demonstrated a good fit between predicted and observed RFS at 1, 3 and 5 years in the training and validation cohorts (Fig. 6b). The clinical-radiomic model performed similarly to the radiomics model in predicting RFS, as evidenced by a comparable C-index of 0.822 (95% CI: 0.805–0.861) in the training cohort. Furthermore, the combined model significantly enhanced the accuracy for predicting RFS with C-index of 0.823 (95% CI: 0.771–0.876) and 0.846 (95% CI: 0.768–0.924) compared to the radiomic and clinical models in the internl and external validation cohort. These results indicate that the nomogram exhibits a good predictive effect for RFS of HCC patients treated with PA-TACE after surgery resection.

Discussion

PA-TACE is an effective strategy to prevent tumor recurrence of patients receiving surgery resection. Specific gene mutations and signatures from next-generation and single-cell sequencing with high cost and invasiveness may serve as potential biomarkers for screening optimal candidates for PA-TACE treatment [28, 29, 30, 31]. However, non-invasive predictive factors are still needed due to lacks effective biomarkers for prognosis [28]. In this study, we developed a multiparametric, MRI-based

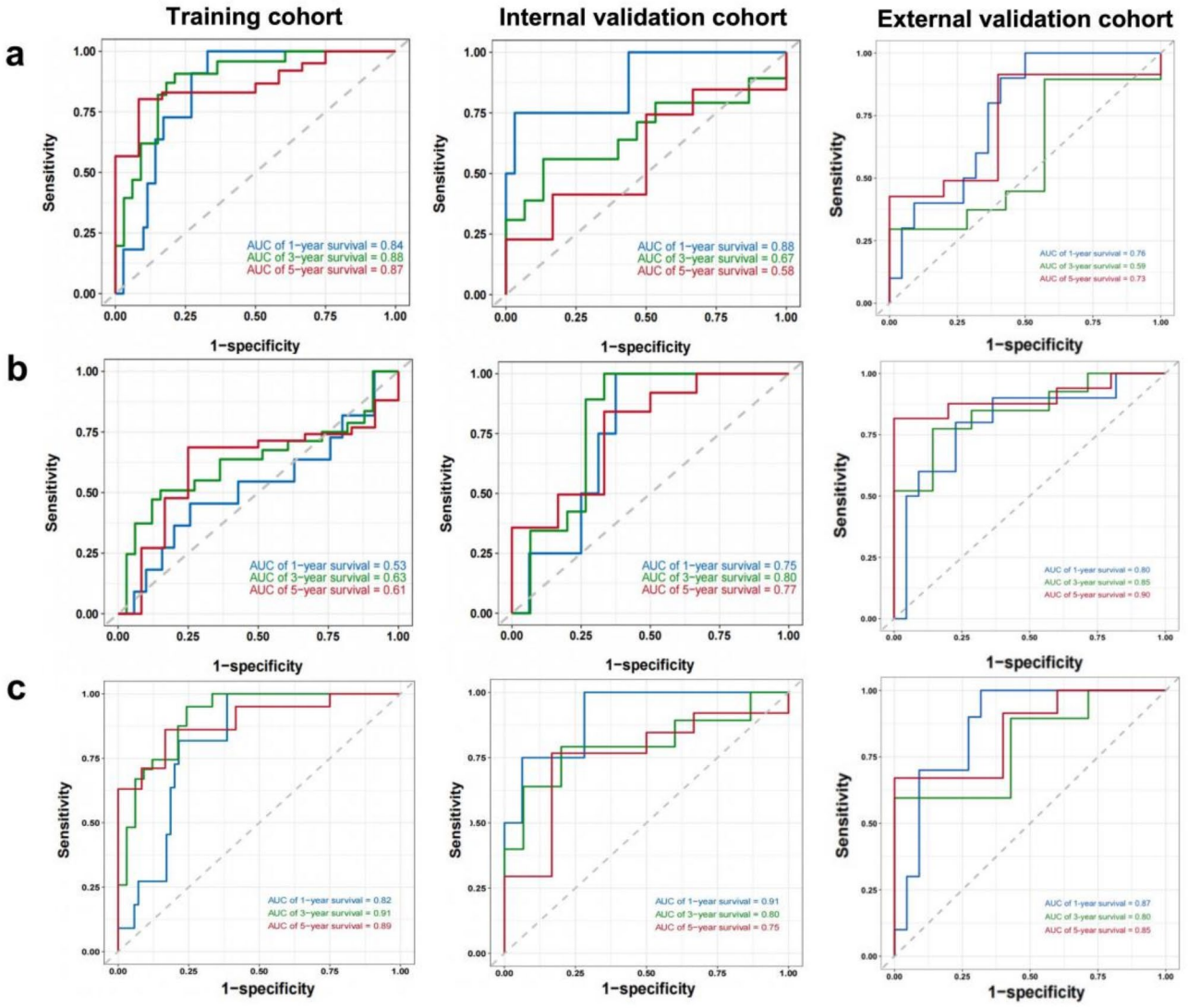

Fig. 5 Time-dependent ROC curves of the three different models in the training and validation cohorts. **(a)** The time-dependent ROC curves based on Rad-score in both the training and cohorts. AUCs at 1-, 3-, and 5-year RFS were calculated from time-dependent ROC curves to evaluate the prognostic accuracy. **(b)** The time-dependent ROC curves based on NLR and tumor size. **(c)** The time-dependent ROC curves based on clinical-radiomics model

radiomics model for predicting recurrence in patients with HCC after PA-TACE and validated it internally. Most of the final radiomic features (8/15) selected to predict HCC recurrence were from wavelet and Laplacian of Gaussian filtered imaging; for example, textural features derived from the grey-level, run-length matrix, which reflects the degree of homogeneity or heterogeneity within tumor regions. High grey levels might be more representative of heterogeneity, such as tumor necrosis and chaotic vascularization. Previous research has demonstrated a correlation between tumor heterogeneity and grey-level features with tumor response and prognosis, findings that are consistent with the results of this study [24, 32, 33]. These results suggest that radiomics has the potential to identify intricate details and extract features from multiparametric MRI scans that are imperceptible or unquantifiable by human observation, thereby providing an accurate reflection of the underlying biology of HCC [22, 34]. The textural features may also serve as indicators of the tumor microenvironment, but further investigation with genomic or histological correlative data is necessary to validate this hypothesis [35]. In our study, these high-dimensional features were further integrated to form the Rad-score, which contained effective biological information and exhibited greater sensitivity in predicting recurrence than clinical features.

Multiple studies have demonstrated the superior performance of Rad-scores in predicting treatment response and prognosis of HCC [14, 22, 24, 36]. Xu et al. developed and validated an MRI-based radiomic model to predict objective response and survival in advanced HCC patients receiving combination therapy with lenvatinib

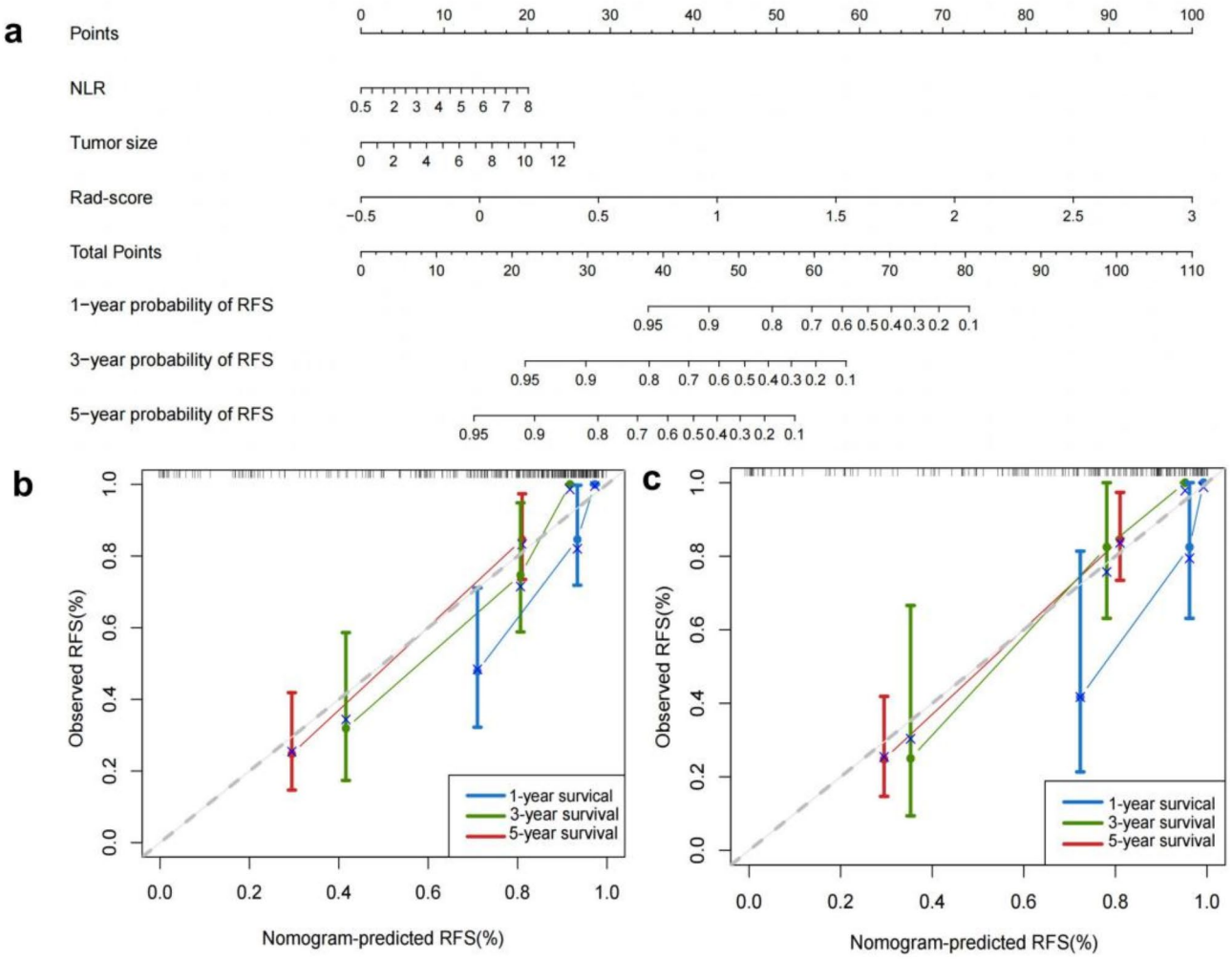

Fig. 6 The nomogram and calibration curves based on the clinical-radiomics model. **(a)** Clinical-Radiomics nomogram for predicting RFS of HCC patients treated with PA-TACE. **(b)** The calibration curves for the Clinical-Radiomics nomogram in both the training and validation cohorts

plus an anti-PD-1 antibody [24]. The results have demonstrated the incremental predictive value of radiomic features beyond clinicopathologic features. The clinicopathologic-radiomic model had a higher AUC in the training (0.987 vs. 0.748) and validation (0.884 vs. 0.702) cohorts compared to the clinicopathologic model. A recent study has also shown that a multi-phase CT radiomics signature was significantly correlated with recurrence following PA-TACE, as evidenced by C-index values of 0.809, 0.812 and 0.892 in training, internal, and external validation cohorts, respectively [14]. Our study further investigated the role of radiomics in multi-phase MRIs, a widely used imaging modality for HCC.

We also confirmed the significance of the NLR and tumor size as crucial prognostic factors for HCC, consistent with previous research findings [24, 37, 38, 39]. The opinion that systemic inflammation, a critical hallmark of cancer, plays a pivotal role in tumor development and progression [37], may account for the higher NLR is related the poor prognosis of HCC. However, the exact mechanism underlying the unfavorable treatment response and survival outcomes observed in patients with an elevated NLR remains unclear, further study is needed. In addition, we also found that the tumor size is the other independent prognostic factor, which is related to tumor burden. Consistent with the six-and-twelve score model, patients with the heavy burden based on tumor diameter and number may serve as a user-friendly tool for stratifying recommended TACE candidates and predicting individual survival with a favorable performance [40]. Notably, we combined these clinical factors and radiomics features to obtain better performance prediction. The AUC of the combined model is much higher than that of the clinical model, indicating that incorporating clinical risk factors into the Rad-score model could add prognostic information that better predicts the risk of recurrence in HCC patients.

Admittedly, this study has several limitations: (1) the sample size was small, and there is potential selection bias due to its retrospective nature; (2) All study participants were diagnosed with hepatitis B virus-related HCC in China; (3) The potential variability across different MRI parameters may still influence the reproducibility of results; (4) Although LASSO regression was employed for feature screening, there remains the possibility of overfitting due to the small sample sizes and high-dimensional features.

In conclusion, we developed and validated a model combined with multiparametric MRI-based radiomics and clinical factors for predicting recurrence in HCC patients treated with PA-TACE. The model demonstrated strong predictive performance in the short term, with AUC values of 0.91 – 0.82 and 0.91 – 0.80 for 1-year and 3-year recurrence, respectively, in all cohorts. However, its performance decreased for 5-year recurrence prediction, with an AUC of 0.75–0.89, indicating room for improvement in long-term prediction. These results suggest that the model is promising for short- to medium-term recurrence prediction, but further optimization and validation are needed to enhance its long-term predictive accuracy.

Abbreviations

AFP	Alpha fetoprotein
AGLR	(ALP [U/L] + GGT[U/L]) /lymphocyte count (×109/L) ratio
AHR	Alanine aminotransferase-to-hemoglobin ratio
BCLC	Barcelona Clinic Liver Cancer
CNLC	China liver cancer staging
GPC3	Glypican-3
Hep	HepPar1
ICCs	Correlation coefficients
LASSO	Least absolute shrinkage and selection operator
MLR	Lymphocyte-monocyte ratio
MRI	Magnetic resonance imaging
NLR	Neutrophil-to-lymphocyte ratio
PACS	Picture Archiving and Communication System
PA-TACE	Postoperative adjuvant transarterial chemoembolization
PLR	Platelet-lymphocyte ratio
RS	Radiomics score
RFS	Recurrence-free survival

Supplementary Information

The online version contains supplementary material available at https://doi.org/10.1186/s12885-025-14079-y.

Supplementary Material 1

Acknowledgements
Not applicable.

Author contributions

Conceptualization, X.Y.G., J.J.S.,and L.Y.Z.; Methodology, X.Y.G., W.Y.C., G.H.L., and L.L.Z.; Software, W.Y.C.; Validation, G.H.L.; Formal analysis, S.L., L.Y.Z, and C.M.H.; Investigation, S.L., L.Y.Z, and C.M.H.; Resources, X.Y.G., and J.J.S.; Data curation, X.Y.G., and J.J.S.; Writing-original draft preparation, X.Y.G. and L.Y.Z.; Writing-review and editing, L.Y.Z.; Visualization, W.Y.C., G.H.L., and L.L.Z; Supervision, Z.W.Z., J.F.T., M.J.C., F.C., and J.S.J.; Project administration, M.J.C., F.C., and J.S.J.; Funding acquisition, W.Y.C. All authors have read and agreed to the published version of the manuscript.

Funding
This study was supported by the Medical and Health Youth Innovation Project of Zhejiang Province (2023RC115).

Data availability

All data generated or analyzed during this study are included in this published article and its supplementary information files.

Declarations

Ethics approval

This retrospective study was received approval by the Ethical Committee of Lishui Hospital of Zhejiang University and was carried out in accordance with the Declaration of Helsinki.

Consent to participate

The requirement for informed consent was waived by the Ethical Committee of Lishui Hospital of Zhejiang University due to the retrospective nature of the research.

Consent for publication

Not applicable.

Competing interests

The authors declare no competing interests.

Author details
[1]Key Laboratory of Imaging Diagnosis and Minimally Invasive Intervention Research, Zhejiang Engineering Research Center of Interventional Medicine Engineering and Biotechnology, Zhejiang Key Laboratory of Imaging and Interventional Medicine, Lishui Hospital of Zhejiang University, Lishui 323000, China
[2]Department of Radiology, The Fifth Affiliated Hospital of Wenzhou Medical University, Lishui 323000, China
[3]Department of Radiology, The First Affiliated Hospital, Zhejiang University School of Medicine, Hangzhou 310003, Zhejiang, China
[4]Second Clinical Medical School, Zhejiang Chinese Medicine University, Hangzhou 310003, Zhejiang, China

Received: 2 March 2024 / Accepted: 3 April 2025
Published online: 14 April 2025

References

1. Sung H, Ferlay J, Siegel RL, et al. Global cancer statistics 2020: GLOBOCAN estimates of incidence and mortality worldwide for 36 cancers in 185 countries. CA Cancer J Clin. 2021;71(3):209–49.
2. Siegel RL, Miller KD, Fuchs HE, et al. Cancer statistics, 2022. CA Cancer J Clin. 2022;72(1):7–33.
3. Imamura H, Matsuyama Y, Tanaka E, Ohkubo T, Hasegawa K, Miyagawa S, Sugawara Y, Minagawa M, Takayama T, Kawasaki S, Makuuchi M. Risk factors contributing to early and late phase intrahepatic recurrence of hepatocellular carcinoma after hepatectomy. J Hepatol. 2003;38(2):200–7.
4. Xu XF, Xing H, Han J, et al. Risk factors, patterns, and outcomes of late recurrence after liver resection for hepatocellular carcinoma: A multicenter study from China. JAMA Surg. 2019;154(3):209–17.
5. Feng X, Feng GY, Tao J, et al. Comparison of different adjuvant therapy regimen efficacies in patients with high risk of recurrence after radical resection of hepatocellular carcinoma. J Cancer Res Clin Oncol. 2023;149(12):10505–18.
6. Yang J, Liang H, Hu K, et al. The effects of several postoperative adjuvant therapies for hepatocellular carcinoma patients with microvascular invasion after curative resection: a systematic review and meta-analysis. Cancer Cell Int. 2021;21(1):92.
7. Luo L, Shan R, Cui L, et al. Postoperative adjuvant transarterial chemoembolisation improves survival of hepatocellular carcinoma patients with microvascular invasion: A multicenter retrospective cohort. United Eur Gastroenterol J. 2023;11(2):228–41.

8. Esagian SM, Kakos CD, Giorgakis E, et al. Adjuvant transarterial chemoembolization following Curative-Intent hepatectomy versus hepatectomy alone for hepatocellular carcinoma: A systematic review and Meta-Analysis of randomized controlled trials. Cancers (Basel). 2021;13(12):2984.
9. Qiu Y, Yang Y, Wang T, et al. Efficacy of postoperative adjuvant transcatheter arterial chemoembolization in hepatocellular carcinoma patients with microscopic portal vein invasion. Front Oncol. 2022;12:831614.
10. Llovet JM, De Baere T, Kulik L, et al. Locoregional therapies in the era of molecular and immune treatments for hepatocellular carcinoma. Nat Rev Gastroenterol Hepatol. 2021;18(5):293–313.
11. Zhang TQ, Su QQ, Huang XY, et al. Micro RNA-4651 serves as a potential biomarker for prognosis when selecting hepatocellular carcinoma patients for postoperative adjuvant transarterial chemoembolization therapy. Hepatol Commun. 2018;2(10):1259–73.
12. Zhao YF, Xiong X, Chen K, et al. Evaluation of the therapeutic effect of adjuvant transcatheter arterial chemoembolization based on Ki67 after hepatocellular carcinoma surgery. Front Oncol. 2021;11:605234.
13. Xu JX, Xing WT, Peng YC et al. Outcomes of postoperative adjuvant transarterial chemoembolization for hepatocellular carcinoma according to the Ki67 index. 2022;18(17): 2113–25.
14. Wang F, Chen Q, Zhang Y, et al. CT-Based radiomics for the recurrence prediction of hepatocellular carcinoma after surgical resection. J Hepatocell Carcinoma. 2022;9:453–65.
15. Hu S, Gan W, Qiao L, et al. A new prognostic algorithm predicting HCC recurrence in patients with Barcelona clinic liver cancer stage B who received PA-TACE. Front Oncol. 2021;11:742630.
16. Xia Z, Zhao Y, Zhao H, et al. Serum Alanine aminotransferase to hemoglobin ratio and radiological features predict the prognosis of postoperative adjuvant TACE in patients with hepatocellular carcinoma. Front Oncol. 2022;12:989316.
17. Sun H, Wang H, Wang Y, et al. Adjuvant transarterial chemoembolization timing after radical resection is an independent prognostic factor for patients with hepatocellular carcinoma. Front Oncol. 2023;13:1129065.
18. Lambin P, Rios-Velazquez E, Leijenaar R, et al. Radiomics: extracting more information from medical images using advanced feature analysis. Eur J Cancer. 2012;48(4):441–6.
19. Huang EP, O'Connor JPB, McShane LM, et al. Criteria for the translation of radiomics into clinically useful tests. Nat Rev Clin Oncol. 2023;20(2):69–82.
20. Bera K, Braman N, Gupta A, et al. Predicting cancer outcomes with radiomics and artificial intelligence in radiology. Nat Rev Clin Oncol. 2022;19(2):132–46.
21. Guiot J, Vaidyanathan A, Deprez L, et al. A review in radiomics: making personalized medicine a reality via routine imaging. Med Res Rev. 2022;42(1):426–40.
22. Kong C, Zhao Z, Chen W, et al. Prediction of tumor response via a pretreatment MRI radiomics-based nomogram in HCC treated with TACE. Eur Radiol. 2021;31(10):7500–11.
23. Chen M, Kong C, Qiao E, et al. Multi-algorithms analysis for pre-treatment prediction of response to transarterial chemoembolization in hepatocellular carcinoma on multiphase MRI. Insights Imaging. 2023;14(1):38.
24. Xu B, Dong SY, Bai XL, et al. Tumor radiomic features on pretreatment MRI to predict response to lenvatinib plus an Anti-PD-1 antibody in advanced hepatocellular carcinoma: A multicenter study. Liver Cancer. 2022;12(3):262–76.
25. Llovet JM, Lencioni R. mRECIST for HCC: performance and novel refinements. J Hepatol. 2020;72(2):288–306.
26. Fang S, Lai L, Zhu J, et al. A radiomics Signature-Based nomogram to predict the Progression-Free survival of patients with hepatocellular carcinoma after transcatheter arterial chemoembolization plus radiofrequency ablation. Front Mol Biosci. 2021;8:662366.
27. Chernyak V, Fowler KJ, Kamaya A, et al. Version 2018: Imaging of Hepatocellular Carcinoma in At-Risk Patients. Radiology. 2018;289(3):816–30. Liver Imaging Reporting and Data System (LI-RADS).
28. Yang C, Zhang H, Zhang L, et al. Evolving therapeutic landscape of advanced hepatocellular carcinoma. Nat Rev Gastroenterol Hepatol. 2023;20(4):203–22.
29. Zhu AX, Abbas AR, de Galarreta MR, et al. Molecular correlates of clinical response and resistance to Atezolizumab in combination with bevacizumab in advanced hepatocellular carcinoma. Nat Med. 2022;28(8):1599–611.
30. Sun Y, Wu L, Zhong Y, et al. Single-cell landscape of the ecosystem in early-relapse hepatocellular carcinoma. Cell. 2021;184(2):404–e42116.
31. Guo L, Yi X, Chen L. Single-Cell DNA sequencing reveals punctuated and gradual clonal evolution in hepatocellular carcinoma. Gastroenterology. 2022;162(1):238–52.
32. Sun R, Limkin EJ, Vakalopoulou M, et al. A radiomics approach to assess tumour-infiltrating CD8 cells and response to anti-PD-1 or anti-PD-L1 immunotherapy: an imaging biomarker, retrospective multicohort study. Lancet Oncol. 2018;19(9):1180–91.
33. Dercle L, Lu L, Schwartz LH, et al. Radiomics response signature for identification of metastatic colorectal cancer sensitive to therapies targeting EGFR pathway. J Natl Cancer Inst. 2020;112(9):902–12.
34. Kang CY, Duarte SE, Kim HS, et al. Artificial Intelligence-based radiomics in the era of Immuno-oncology. Oncologist. 2022;27(6):e471–83.
35. Dong D, Fang MJ, Tang L, et al. Deep learning radiomic nomogram can predict the number of lymph node metastasis in locally advanced gastric cancer: an international multicenter study. Ann Oncol. 2020;31(7):912–20.
36. Ji GW, Zhu FP, Xu Q, et al. Radiomic features at Contrast-enhanced CT predict recurrence in early stage hepatocellular carcinoma: A Multi-Institutional study. Radiology. 2020;294(3):568–79.
37. Nøst TH, Alcala K, Urbarova I, et al. Systemic inflammation markers and cancer incidence in the UK biobank. Eur J Epidemiol. 2021;36(8):841–8.
38. Schobert IT, Savic LJ, Chapiro J, et al. Neutrophil-to-lymphocyte and platelet-to-lymphocyte ratios as predictors of tumor response in hepatocellular carcinoma after DEB-TACE. Eur Radiol. 2020;30(10):5663–73.
39. Mao S, Shan Y, Yu X, et al. A new prognostic model predicting hepatocellular carcinoma early recurrence in patients with microvascular invasion who received postoperative adjuvant transcatheter arterial chemoembolization. Eur J Surg Oncol. 2023;49(1):129–36.
40. Wang Q, Xia D, Bai W, et al. Development of a prognostic score for recommended TACE candidates with hepatocellular carcinoma: A multicentre observational study. J Hepatol. 2019;70(5):893–903.

Publisher's note